GeroScience (2020) 42:595–611
https://doi.org/10.1007/s11357-020-00166-4

ORIGINAL ARTICLE

CD82-TRPM7-Numb signaling mediates age-related cognitive impairment

Yin Zhao · Tamas Kiss · Jordan DelFavero · Lu Li · Xing Li · Lu Zheng · Jie Wang · Chao Jiang · Jing Shi · Zoltan Ungvari · Anna Csiszar · Xin A. Zhang

Received: 27 August 2019 / Accepted: 4 October 2019 / Published online: 22 February 2020

Abstract Aging is a crucial cause of cognitive decline and a major risk factor for Alzheimer's disease (AD); however, AD's underlying molecular mechanisms remain unclear. Recently, tetraspanins have emerged as important modulators of synaptic function and memory. We demonstrate that the level of tetraspanin CD82 is upregulated in the brains of AD patients and middle-aged mice. In young adult mice, injection of AAV-CD82 to the hippocampus induced AD-like cognitive deficits and impairments in neuronal spine density. CD82 overexpression increased TRPM7 α-kinase cleavage via caspase-3 activation and induced Numb phosphorylation at Thr346 and Ser348 residues. CD82 overexpression promoted beta-amyloid peptide (Aβ) secretion which could be reversed by Numb T346S348 mutants. Importantly, hippocampus-related memory functions were improved in *Cd82*$^{-/-}$ mice. Taken together, our findings provide the evidence that links the elevated CD82-TRPM7-Numb signaling to age-related cognitive impairment.

Keywords Alzheimer's disease · Memory · CD82 · TRPM7 α-kinase · Numb

Y. Zhao (✉) · L. Li
Department of Ophthalmology, Tongji Hospital, Tongji Medical College, Huazhong University of Science and Technology, Wuhan 430030, China
e-mail: Yin.Zhao@ucsf.edu

T. Kiss · J. DelFavero · Z. Ungvari · A. Csiszar
Vascular Cognitive Impairment and Neurodegeneration Program, Reynolds Oklahoma Center on Aging, Department of Geriatrics, University of Oklahoma Health Sciences Center, Oklahoma City 73104, USA

X. Li · L. Zheng · J. Shi
Department of Neurobiology, Key Laboratory of Neurological Diseases, Ministry of Education, Tongji Medical College, Huazhong University of Science and Technology, Wuhan 430030, China

X. Li · L. Zheng · J. Shi
The Institute for Brain Research, Collaborative Innovation Center for Brain Science, Huazhong University of Science and Technology, Wuhan 430030, China

J. Wang · C. Jiang · X. A. Zhang (✉)
Stephenson Cancer Center and Department of Physiology, University of Oklahoma Health Sciences Center, Oklahoma City 73104, USA
e-mail: xin-zhang-1@ouhsc.edu

Introduction

Alzheimer's disease (AD) is a devastating neurodegenerative disease with progressive impairment of memory and is the most frequent type of human dementia worldwide (Graham et al. 2017). The neuropathological hallmarks of the disease are extracellular senile plaques composed of beta-amyloid peptide (Aβ) and intracellular neurofibrillary tangles composed of hyperphosphorylated Tau protein (Forner et al. 2017), which lead to severe neuronal loss. To better understand the disease, findings from the well-studied molecular biochemistry of Aβ must be integrated into the complex cellular context of the neural system.

Tetraspanins are a family of proteins with four transmembrane domains that play a role in many aspects of physiology and pathology (Charrin et al. 2014). Tspan7 is involved in synapse development and interacts with PICK1 in the postsynaptic density complex, which regulates trafficking of AMPA receptors (Bassani et al. 2012). Tspan6 overexpression in cells increases Aβ level (Guix et al. 2017). However, *Tspan6*-knockout mice show no defects in hippocampus-dependent memory tests (Salas et al. 2017). Tspan27 (CD82) regulates the signaling of membrane molecules by altering their subcellular distributions and suppresses the progression and metastasis of solid malignant tumors (Feng et al. 2015). The role and function of CD82 in the neural system, especially in AD, are unclear.

Transient receptor potential melastatin-like 7 (TRPM7) is a member of the transient receptor potential (TRP) channel family that contains a C-terminal α-kinase domain, which recognizes substrates with alpha-helical conformation (Fleig and Chubanov 2014). TRPM7 is cleaved by caspase-3 at D1510, disassociating the α-kinase domain from the channel (Desai et al. 2012). Previous work has shown that TRPM7 knockdown in the hippocampus impairs learning and memory and reduces synaptic density and plasticity in adult rats. Restoring expression of the α-kinase domain rescues memory and synaptic density/plasticity by phosphorylating cofilin (Liu et al. 2018). TRPM7 α-kinase can phosphorylate annexin-A1 and myosin IIA (Visser et al. 2014), although its natural substrates are unclear. Our previous study found that annexin-A1 and myosin IIA phosphorylated by TRPM7 α-kinase impairs learning and memory ability in rats after ischemic stroke (Zhao et al. 2015).

Numb is an adaptor protein that interacts with Notch and inhibits Notch signaling (Chan et al. 2002). Numb regulates the transport and processing of the amyloid precursor protein (APP) with an amino-terminal phosphotyrosine-binding domain (Yap and Winckler 2015). RNAi knockdown of Numb decreases Aβ secretion (Xie et al. 2012).

In the present study, we report that CD82 levels are increased in brains of AD patients and of middle-aged mouse model. CD82 overexpression in the hippocampus impairs learning, memory, and synaptic plasticity in young adult mice. We show that CD82 enhances TRPM7 α-kinase cleavage via caspase-3 activation. TRPM7 α-kinase increases Numb phosphorylation at Thr 346 and Ser 348 residues. CD82 increases Aβ secretion in a Numb phosphorylation-dependent manner. *Cd82*$^{-/-}$ mice show improved long-term memory in the radial arm water maze test and Y-maze test. Our findings strongly indicate a pathophysiological role for CD82 in the development of AD and its potential as a novel AD therapy target.

Experimental procedure

Animals

Three-month-old young adult and 14.5-month-old middle-aged male C57BL/6J mice (Fahlstrom et al. 2011; Shoji and Miyakawa 2019) were obtained from the Experiment Animal Center of the Tongji Medical College, Huazhong University of Science and Technology, China.

The establishment of the *Cd82*$^{-/-}$ mouse line and the mouse genotyping strategy was described previously (Wei et al. 2014). All the animals used in the radial arm water maze, Y-maze, accelerating rotarod, and grip strength tests were born in December 2018. Ten female and 15 male mice with ages between 5 and 6 months were used for the study.

All animal experiments were approved by the Ethics Committees for Animal Experimentation of Huazhong University of Science and Technology and the University of Oklahoma Health Sciences Center in strict accordance with the Guide for the Care and Use of Laboratory Animals published by the U.S. National Institutes of Health. Efforts were made to minimize animal suffering and to reduce the number of animals used.

Human brain samples

Brain tissues from normal control subjects and AD patients were obtained from the Chinese Brain Bank Center (Wuhan, China). Diagnoses of AD were confirmed by the presence of amyloid plaques and neurofibrillary tangles in formalin-fixed tissue. This study was performed in accordance with the principles of the Declaration of Helsinki and approved by the Ethics Committee of Tongji Hospital, Tongji Medical College, HUST, China (2017-K-036). The information of the human case materials is listed in Table 1.

Table 1 Human brain tissues used in the study

Case number	Age at death	Sex	Braak score	Final diagnosis	ApoE
Control l	73	M	Braak I	Liver cancer	ApoE3/3
Control 2	84	M	Braak I	Heart failure	ApoE3/3
Control 3	76	F	Braak I	Breast cancer	ApoE3/3
Control 4	69	M	Braak II	Myocardial infarct	ApoE3/3
AD 1	72	F	Braak VI	AD	ApoE3/4
AD 2	79	M	Braak VI	AD	ApoE3/4
AD 3	75	M	Braak VI	AD	ApoE4/4
AD 4	70	M	Braak VI	AD	ApoE3/4

Reagents and antibodies

The caspase inhibitor Z-VAD-FMK was obtained from Selleckchem (50 μmol/L, Houston, TX). The proteasome inhibitor MG 132 was also procured from Selleckchem (1 μM, S2619, Houston, TX). The lysosome inhibitor hydroxychloroquine sulfate (HCQ) was purchased from Selleckchem (20 μM, S4430, Houston, TX).

All antibodies used in the study are listed in Table 2.

ELISA

Sandwich ELISA was performed to measure the levels of Aβ42 and Aβ40 in N2a/APP cell (N2a stably transfected with amyloid precursor protein cell lines) (Wang et al. 2008) by using the V-PLEX Aβ Peptide Panel 1 (4G8) Kit (Meso Scale Discovery, Rockville, MD) according to the manufacturer's instruction.

Plasmids and viruses

Human full-length CD82 was cloned into pCDNA3.1-HA vector. Mouse Numb T346S348A plasmid was generated using PCR-based site-directed mutagenesis procedures. All plasmids were constructed and purified by Genewiz, Inc. (Suzhou, China). Mouse CD82 was cloned into rAAV-hsyn-mCherry-WPRE-pA vector by BrainVTA, Inc. (Wuhan, China).

Morris water maze

The Morris water maze test was performed as previously described (Zhao et al. 2015). Briefly, mice were trained for five consecutive days to find a platform hidden 1 cm underwater, using a stationary array of cues on the walls. A digital tracking device was connected to a computer and was used to track the movement of mice in the pool. The escape latency of mice to reach the hidden platform was detected. On the sixth day, mice received bilateral intrahippocampal AAV injection (CA3 field of the hippocampus, anterior/posterior = ± 1.9 mm, medial/lateral = ± 1.9 mm, dorsal/ventral = ± 2.4 mm) and rested for 14 days. From the 20th day to the 24th day, the mice underwent five consecutive days of training to find the platform. On the 24th day, the hidden platform was removed, the latency to reach the place of platform and swimming velocity were measured, and the percent time spent in the target quadrant was recorded.

Radial arm water maze test

Hippocampus-related spatial memory and long-term memory were examined with radial arm water maze test (RAWM test) as previously described (Ungvari et al. 2017). A special, eight-arm maze was filled with water mixed with white food coloring. A hidden, underwater escape platform was placed at the end of one arm. Visual clues were placed at the end of each arm to help the animals. In each trial, the animal had 1 min to find the escape platform. The RAWM test has three segments, learning, probe, and reversal. In learning phase, animals are tested eight times a day for three consecutive days. Seven days later, during the probe phase, the animals are tested again, four times in 1 day. During the learning and probe phases, the location of the escape platform remains the same. In the reversal phase, the location of the platform is changed while the orientation of the maze with the clues stays the same. During the reversal phase,

Table 2 The antibodies used in the study

Antigen	Source	Cat number	Type	WB	IF	IHC
NeuN	Millipore	MAB377	mAb		1:250	
Iba1	Abcam	ab5076	pAb		1:200	
TRPM7	Abcam	ab109438	mAb	1:1000		
Human CD82	Abcam	ab59509	mAb		1:100	1:50
Murine CD82	Karafast	M35	pAb	1:200		
Cleaved caspase-3	Cell Signaling	No. 9664	mAb	1:1000		
Phospho-Ser/-Thr	Cell Signaling	No. 9631	pAb	1:100 (IP)		
Numb	Abcam	ab4147	pAb	1:1000		
β-Actin	Santa Cruz	sc-47778	mAb	1:1000		

the animals are tested eight times in 1 day. During the trials, movement of each animal is recorded and analyzed by a standalone video tracking system (EthoVision XT by Noldus Information Technology Inc., Leesburg, VA, USA).

Y-maze test

Hippocampus-related memory is tested by the Y-maze test, as previously described (Valcarcel-Ares et al. 2019). The Y-maze test has two segments: learning and probe phases. The animals are placed into the start arm of a special, 3 armed, Y-shaped maze. Visual clues are placed at the end of each arm. During the learning, one arm was completely closed from the others (novel arm) and the animals had 5 min to explore the start and the familiar arms. Four hour later, the probe is performed. The wall, closing the novel arm, is removed and the animals are placed at the same start arm to explore the maze for 2 min. During the trials, the movement of the animals is recorded and analyzed by a standalone video tracking system (EthoVision XT by Noldus Information Technology Inc., Leesburg, VA, USA).

Accelerating rotarod test

Balance and motor skills were assessed by the accelerating rotarod test as it was previously described (Tarantini et al. 2018). During a 4-day-long experimental period, the animals are placed on a special rotating wheel (Rotamex, Columbus Instruments Inc., Columbus, OH, USA) three times a day. During each session, the speed of the rotation increased gradually until the animals could not keep up with the rotation and fell off the wheel. Time of termination is recorded.

Grip strength test

To evaluate in vivo muscle strength and endurance, we determined forelimb grip strength using an electronic pull strain gauge (Chatillon Digital Force Gauge DFIS 2, AMETEK Inc., Berwyn, PA, USA) as previously described (Tarantini et al. 2018). The test was performed by the same observer three consecutive times.

Co-immunoprecipitation analysis

Cell lysates (600 μg of protein) were diluted fourfold with IP buffer (Beyotime Institute of Biotechnology) containing protease inhibitor cocktail. The samples were precleared for 1 h with 10 μl of protein A/G PLUS-Agarose beads (Santa Cruz Biotechnology) and were then centrifuged to remove proteins that adhered non-specifically to the protein A/G beads. The supernatant was incubated with 2 μg of anti-phosS/TP antibody or control IgG with gentle rotation overnight at 4 °C. Thereafter, 20 μl of protein A/G PLUS-Agarose beads was added, and the samples were incubated at 4 °C for an additional 4 h. The precipitates were washed three times with IP buffer, denatured in 30 μl loading buffer, boiled at 95 °C in a block heater (ThermoFisher Scientific), and subjected to SDS-PAGE.

Western blotting and Immunostaining

In brief, equivalent amounts of total protein were subjected to 10 or 12% sodium dodecyl sulfate-

polyacrylamide gel electrophoresis (SDS-PAGE) and were transferred to polyvinylidene difluoride (PVDF) membranes (Millipore).

For immunofluorescence staining, coronal sections were gently rinsed twice with PBS solution, permeabilized with 0.5% Triton X-100 for 60 min, and blocked with 10% donkey serum for an additional 60 min. The sections were then incubated with antigen-specific primary antibodies overnight at 4 °C. The samples were then rinsed thoroughly three times in 0.25% Tween-20 in PBS and incubated with secondary antibodies at room temperature for 60 min. The cells were examined and counted immediately under fluorescence microscopy (IX73, Olympus, Tokyo, Japan).

For immunohistochemistry analysis, tissue sections were deparaffinized in xylene and rehydrated through descending concentrations of ethanol. The endogenous peroxidase activity was eliminated by incubation in 3% hydrogen peroxide in methanol for 5 min. After antigen-retrieval in boiling sodium citrate buffer (10 mM), the sections were incubated with primary antibody at 4 °C for overnight and peroxidase-conjugated secondary antibody at room temperature for 2 h. The signal was developed using Histostain-SP kit (Invitrogen).

Isobaric tags for relative and absolute quantitation labeling and LC-MS/MS analysis

HEK293 cells and HEK293 cells transfected with human TRPM7 α-kinase domain plasmids and CD82 plasmids in lysis buffer (8 M urea, 1% protease inhibitor cocktail) were sonicated three times on ice using a high-intensity ultrasonic processor (Scientz). The remaining debris was removed by centrifugation at 12,000*g* at 4 °C for 10 min. Finally, the supernatant was collected and the protein concentration was determined with a BCA kit according to the manufacturer's instructions. For digestion, the protein solution was reduced with 5 mM dithiothreitol for 30 min at 56 °C and alkylated with 11 mM iodoacetamide for 15 min at room temperature in the dark. The protein sample was diluted by adding 100 mM TEAB to achieve a urea concentration of less than 2 M. Finally, trypsin was added at 1:50 trypsin-to-protein mass ratio for the first digestion overnight and 1:100 trypsin-to-protein mass ratio for a second 4-h digestion. After trypsin digestion, peptide was desalted by Strata X C18 SPE column (Phenomenex) and vacuum-dried. Peptides were reconstituted in 0.5 M TEAB and processed according to the manufacturer's protocol for isobaric tags for relative and absolute quantitation (iTRAQ) kit. Briefly, one unit of iTRAQ reagent was thawed and reconstituted in acetonitrile. The peptide mixtures were then incubated for 2 h at room temperature and were pooled, desalted, and dried by vacuum centrifugation. Tryptic peptides were fractionated into fractions by high pH reverse-phase HPLC using Thermo Betasil C18 column (5-μm particles, 10 mm i.d., 250 mm length). Briefly, peptides were first separated into 60 fractions with a gradient of 8 to 32% acetonitrile (pH 9.0) over 60 min. Then, the peptides were combined into fractions and dried by vacuum centrifuging. To enrich modified peptides, tryptic peptides dissolved in NETN buffer (100 mM NaCl, 1 mM EDTA, 50 mM Tris-HCl, 0.5% NP-40, pH 8.0) were incubated with pre-washed antibody beads (Lot number PTM-703, PTM Bio) at 4 °C overnight with gentle shaking. The beads were washed four times with NETN buffer and twice with H_2O. The bound peptides were eluted from the beads with 0.1% trifluoroacetic acid. Finally, the eluted fractions were combined and vacuum-dried.

For LC-MS/MS analysis, the resulting peptides were desalted with C18 ZipTips (Millipore) according to the manufacturer's instructions. Peptide mixtures were first incubated with IMAC microsphere suspension with vibration in loading buffer (50% acetonitrile/6% trifluoroacetic acid). The IMAC microspheres with enriched phosphopeptides were collected by centrifugation, and the supernatant was removed. To remove non-specifically adsorbed peptides, the IMAC microspheres were washed with 50% acetonitrile/6% trifluoroacetic acid and 30% acetonitrile/0.1% trifluoroacetic acid, sequentially. To elute the enriched phosphopeptides from the IMAC microspheres, elution buffer containing 10% NH_4OH was added, and the enriched phosphopeptides were eluted with vibration. The supernatant containing phosphopeptides was collected and lyophilized for LC-MS/MS analysis. The tryptic peptides were dissolved in 0.1% formic acid (solvent A), directly loaded onto a home-made reversed-phase analytical column (15 cm length, 75 μm i.d.). The gradient

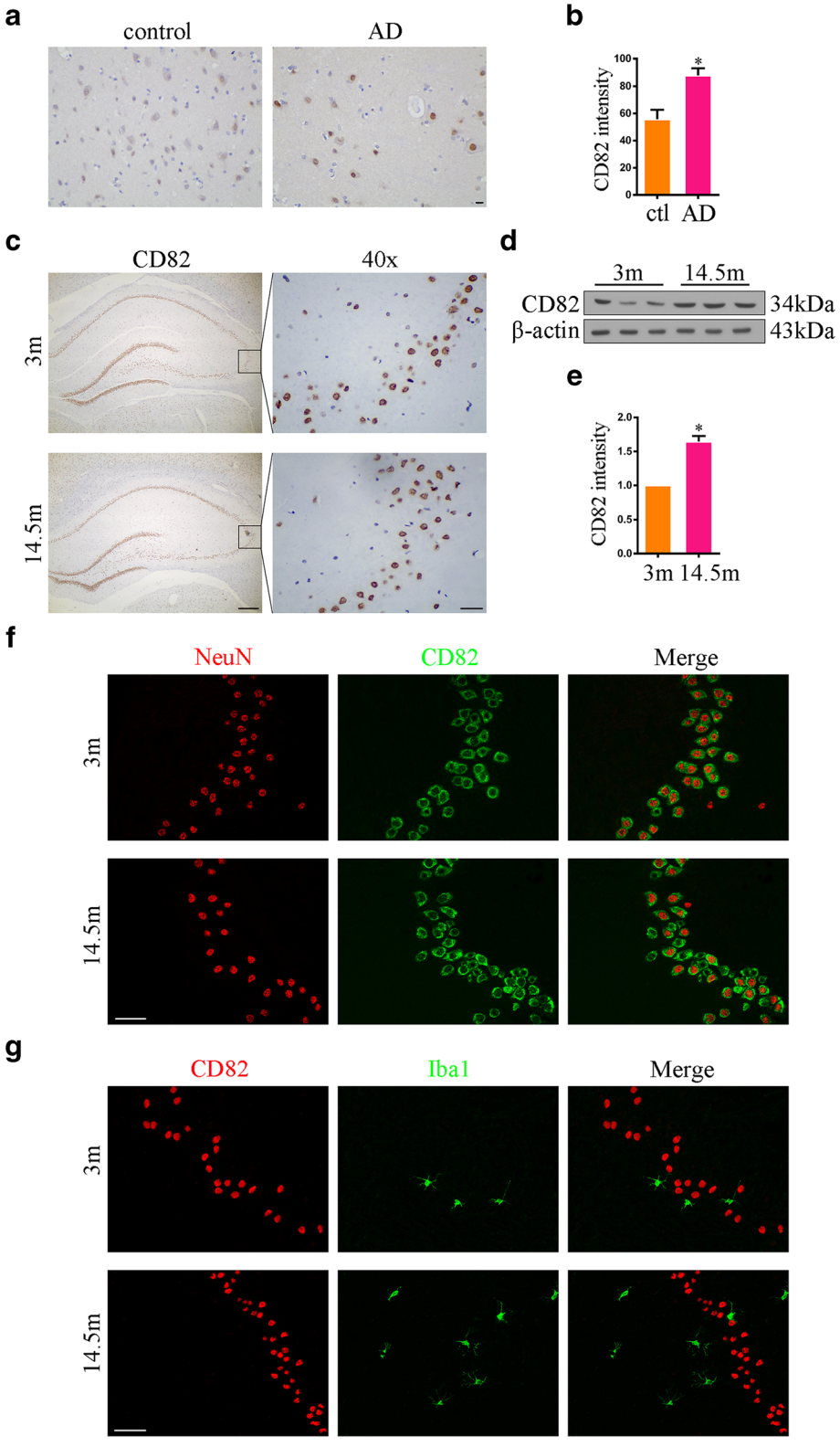
a
control
AD
b
CD82 intensity
ctl AD
c
CD82
40x
3m
14.5m
d
3m 14.5m
CD82
β-actin
34kDa
43kDa
e
CD82 intensity
3m 14.5m
f
NeuN
CD82
Merge
3m
14.5m
g
CD82
Iba1
Merge
3m
14.5m

◀ **Fig. 1** CD82 is increased in the brains of patients with Alzheimer's disease (AD) and middle-aged model mice. **a** Representative immunohistochemistry images of CD82 expression in cortex samples of AD patients (scale bars, 10 μm; $n = 3$). **b** Statistical analysis of **a**. The data are presented as mean ± S.E.M. Unpaired Student's t test was used, $*p < 0.05$ versus control. **c** Representative immunohistochemical images of CD82 expression in aged mouse hippocampal section (left scale bars, 200 μm; right scale bars, 50 μm; $n = 6$). **d** Western blot analysis, showing the expression of CD82 in mouse hippocampal extract ($n = 3$). **e** Statistical analysis of **d**. The data are presented as mean ± S.E.M. Unpaired Student's t test was used, $*p < 0.05$ versus control. **f** Immunofluorescence analysis, showing the expression of CD82 in CA3 hippocampus domain in mice (scale bars, 50 μm; $n = 6$). Representative results from three independent experiments are shown (red: NeuN; green: CD82). **g** Immunofluorescence analysis, showing the expression of CD82 in the CA3 hippocampus domain in mice (scale bars, 50 μm; $n = 6$). Representative results from three independent experiments are shown (red: CD82; green: Iba1)

was comprised of an increase from 6 to 23% solvent B (0.1% formic acid in 98% acetonitrile) over 26 min, 23 to 35% over 8 min, climbing to 80% in 3 min then holding at 80% for the last 3 min, all at a constant flow rate of 400 nL/min on an EASY-nLC 1000 UPLC system.

The peptides were subjected to NSI source followed by tandem mass spectrometry (MS/MS) in Q Exactive™ Plus (Thermo) coupled online to the UPLC. The electrospray voltage applied was 2.0 kV. The m/z scan range was 350 to 1800 for the full scan. Intact peptides were detected in the Orbitrap at a resolution of 70,000. Peptides were then selected for MS/MS using 28 as the NCE setting, and the fragments were detected in the Orbitrap at a resolution of 17,500. A data-dependent procedure that alternated between one MS scan followed by 20 MS/MS scans with 15.0-s dynamic exclusion was performed. Automatic gain control (AGC) was set at 5E4. Fixed first mass was set as 100 m/z.

Statistical analysis

All values are expressed as the mean ± S.E.M. of at least three independent experiments. The data were analyzed using GraphPad Prism (version 6.03, GraphPad Software, Inc.). Differences between two groups were assessed using Student's unpaired t test (two-tailed). The variance among multiple groups was determined by one-way or two-way ANOVA with/without repeated measures, followed by the Newman-Keuls test. A value of $p < 0.05$ was considered to indicate statistical significance.

Results

CD82 expression levels are increased in the brains of AD patients and middle-aged mice

To evaluate a potential pathophysiological role of CD82 in human AD, we detected the protein levels of CD82 in AD patient brains. Notably, we found that CD82 expression levels were increased in the frontal cortex in AD human brains compared with age-matched controls (Fig. 1a, b). We found that compared with 3-month-old young adult mice, the expression of CD82 was increased in the hippocampus CA3 region in 14.5-month-old middle-aged mice (Fig. 1c). We also examined the expression of CD82 in hippocampus extracts. Western blotting results revealed that the expression of CD82 in middle-aged mouse hippocampus extract was increased (Fig. 1d, e). As shown in Fig. 1f, CD82 was mainly present in hippocampus CA3 neuron cells in mice (Fig. 1f). By contract, we found no colocalization with microglia marker Iba1 (Fig. 1g). These findings suggest that the expression of CD82 was increased in the brains of AD patients, compared with non-AD humans, and of middle-aged mice, compared with young mice.

CD82 overexpression impairs learning and memory in young adult mice

To investigate the impact of increased CD82 on hippocampus-dependent cognitive behavior, we performed bilateral intrahippocampal injection of AAV-vector (AV) or AAV-CD82 (AC) virus to 3-month-old young adult C57/BL6 mice (Fig. 2a). Overexpression of CD82-mcherry in the hippocampus CA3 region was confirmed by fluorescence microscopy 14 days after injection (Fig. 2b). Overexpression of CD82 in hippocampus extract was confirmed by western blot (Fig. 2c, d).

In the Morris water maze test, all mice received five consecutive days of training to find a platform. The escape latency of mice to reach the hidden platform was detected. The analysis

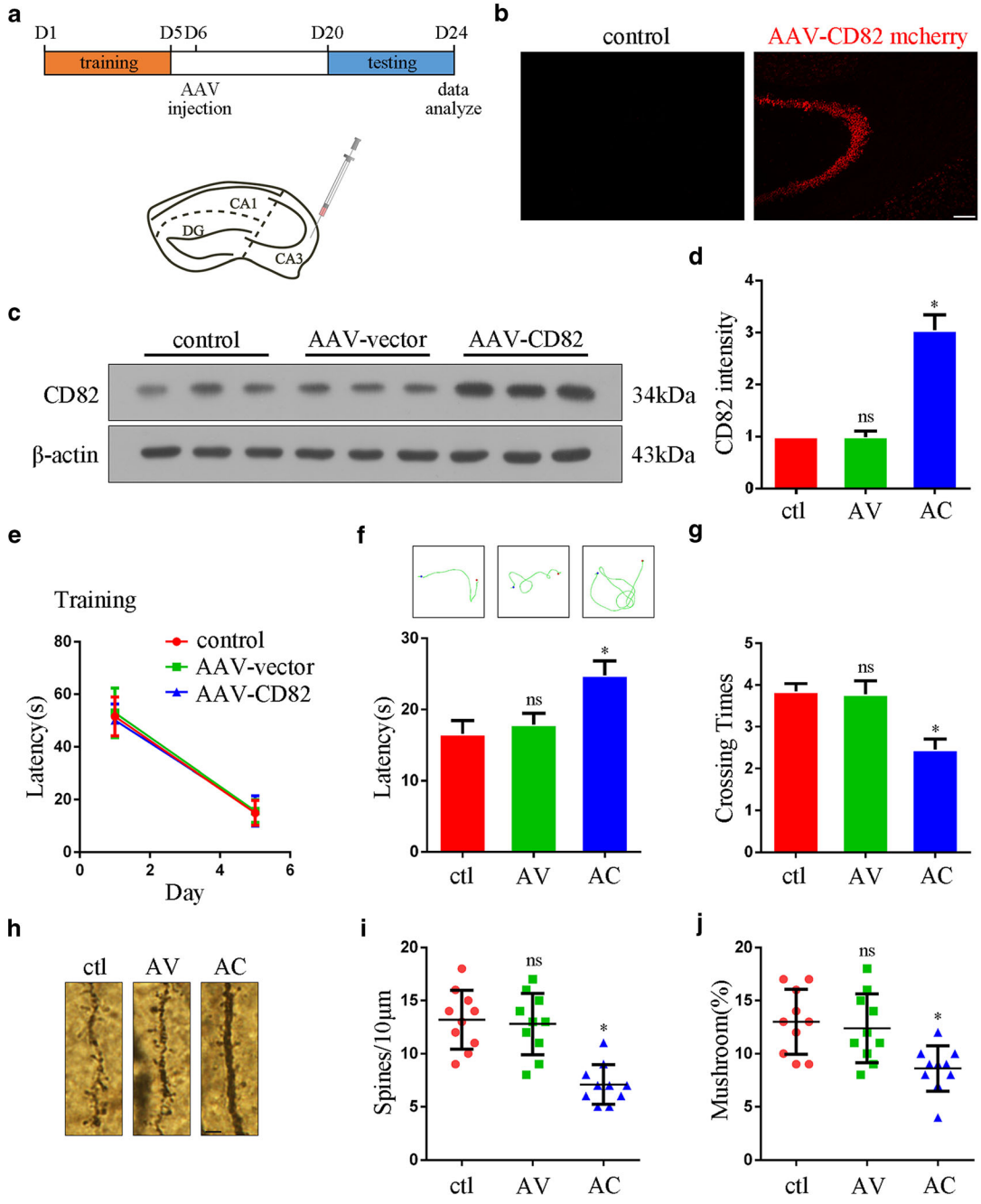

showed no significant difference in escape latency on day 5 between the control group, AAV-vector injection group, and AAV-CD82 injection group mice (Fig. 2e). The impact of CD82 overexpression on cognitive behavior was analyzed on the twenty-fourth day. CD82 overexpression increased escape latency and decreased crossing times in young adult mice (Fig. 2f, g). Golgi staining showed that CD82 overexpression promoted decrease of dendritic spine (Fig. 3h, j). Together, these results indicate that CD82 induces learning and memory deficits.

◀ **Fig. 2** Increased CD82 impaired behavioral and morphological changes in a young adult mouse model. **a** Three-month-old mice were trained to search for the platform from day 1 to day 5 and received CD82 AAV injection on day 6. From day 20 to day 24, mice performed the platform searching test in the Morris water maze. **b** Immunofluorescence analysis, showing the expression of mCherry in the hippocampus. Representative results from three independent experiments are shown (scale bars, 100 μm; red: mCherry). **c** Western blot analysis, showing the expression of CD82 in mouse hippocampus extract ($n = 3$). **d** Statistical analysis of **c**. The data are presented as mean ± S.E.M. Unpaired Student's t test was used, $^*p < 0.05$ versus control. **e** Three-month-old mice were injected with AAV-CD82 (AC) or control AAV (AV) into CA3 of the hippocampus, and 3-month-old uninjected mice as age-matched control mice (ctl). The latency to reach a hidden platform on days 1 and 5 was recorded. Two-way analysis of variance (ANOVA) with repeated measures was used for interaction effect. $n = 8$ for each group. **f** The latency to reach a hidden platform area on day 24. One-way ANOVA with Bonferroni post hoc test was used. ns $p > 0.05$ compared with control; $^*p < 0.05$ compared with AV. $n = 8$ for each group. **g** The crossing time for hidden platform area on day 24. One-way ANOVA with Bonferroni post hoc test was used. ns $p > 0.05$ compared with control; $^*p < 0.05$ compared with AV. $n = 8$ for each group. **h** Golgi staining of 3-month-old mice injected with AAV-CD82 or control AAV (scale bars, 10 μm). The images were taken using a microscope (Nikon, Tokyo, Japan). **i**–**j** Statistical analysis of **h**. Fifteen images were randomly chosen for each group ($n = 6$). One-way ANOVA with Bonferroni post hoc test was used. ns $p > 0.05$ compared with control; $^*p < 0.05$ compared with AV

CD82 overexpression promotes TRPM7 α-kinase cleavage

To examine whether CD82 participates in memory regulation via TRPM7, we transfected HEK293 cells with CD82 full-length plasmids. We found that CD82 overexpression resulted in an increase in cleaved caspase-3 and cleaved TRPM7 (42 kDa) (Fig. 3a). Caspase inhibitor Z-VAD-FMK reduced TRPM7 cleavage (Fig. 3b). However, proteasome inhibitor (MG 132) or lysosome inhibitor (HCQ) could induce TRPM7 cleavage under CD82 overexpression conditions (Fig. 3c). These results suggest that CD82 overexpression induced caspase-3 activation, which is responsible for increased cleavage of TRPM7 α-kinase, and that TRPM7 α-kinase cleavage was independent of proteasomal and/or lysosomal pathways.

TRPM7 α-kinase induces Numb phosphorylation

Because TRPM7 α-kinase function is unclear in AD, HEK293 cells were transfected with TRPM7 α-kinase domain plasmids, and the samples were subjected to a high-throughput quantitative proteome analysis using iTRAQ (Fig. 4a). As shown in Fig. 4b, we identified 3347 proteins (3079 protein localization probability > 0.75) and 10,060 phosphorylation sites (7751 site localization probability > 0.75). We quantified 2621 proteins (2468 protein localization probability > 0.75) and 6422 phosphorylation sites (5510 site localization probability > 0.75). Abundance of 131 phosphorylation sites and 112 proteins increased (fold change > 1.5), while abundance of 108 phosphorylation sites and 92 proteins decreased (fold change > 1.5) in response to TRPM7 α-kinase overexpression. According to fold change in response to TRPM7 α-kinase overexpression, we separated the altered proteins into four groups (Q1 to 4). Group Q1 included proteins with fold change from 0 to

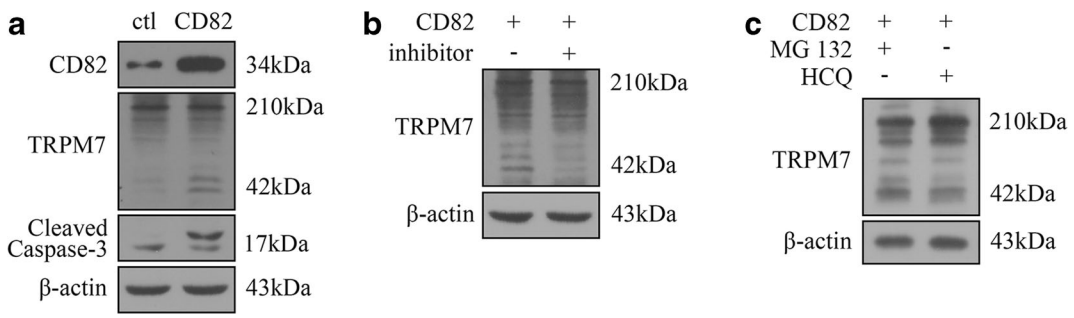

Fig. 3 Increased CD82 induced cleavage of TRPM7 to release the kinase domain. **a** HEK293 cells were transfected with full-length human CD82 plasmid. Western blot analysis, showing the expression of CD82, TRPM7, and cleaved caspase-3 after CD82 overexpression ($n = 3$). **b** Fifty micromole per liter caspase inhibitor Z-VAD-FMK was incubated into HEK293 cells 6 h before plasmid transfection. Western blot analysis, showing the expression of TRPM7 ($n = 3$). **c** HEK293 cells were incubated with 1 μM proteasome inhibitor MG132 and 20 μM lysosome inhibitor hydroxychloroquine sulfate (HCQ) 6 h before plasmid transfection. Western blot analysis, showing the expression of TRPM7 ($n = 3$). **d** Co-IP results demonstrated the binding between CD82 and TRPM7 ($n = 3$)

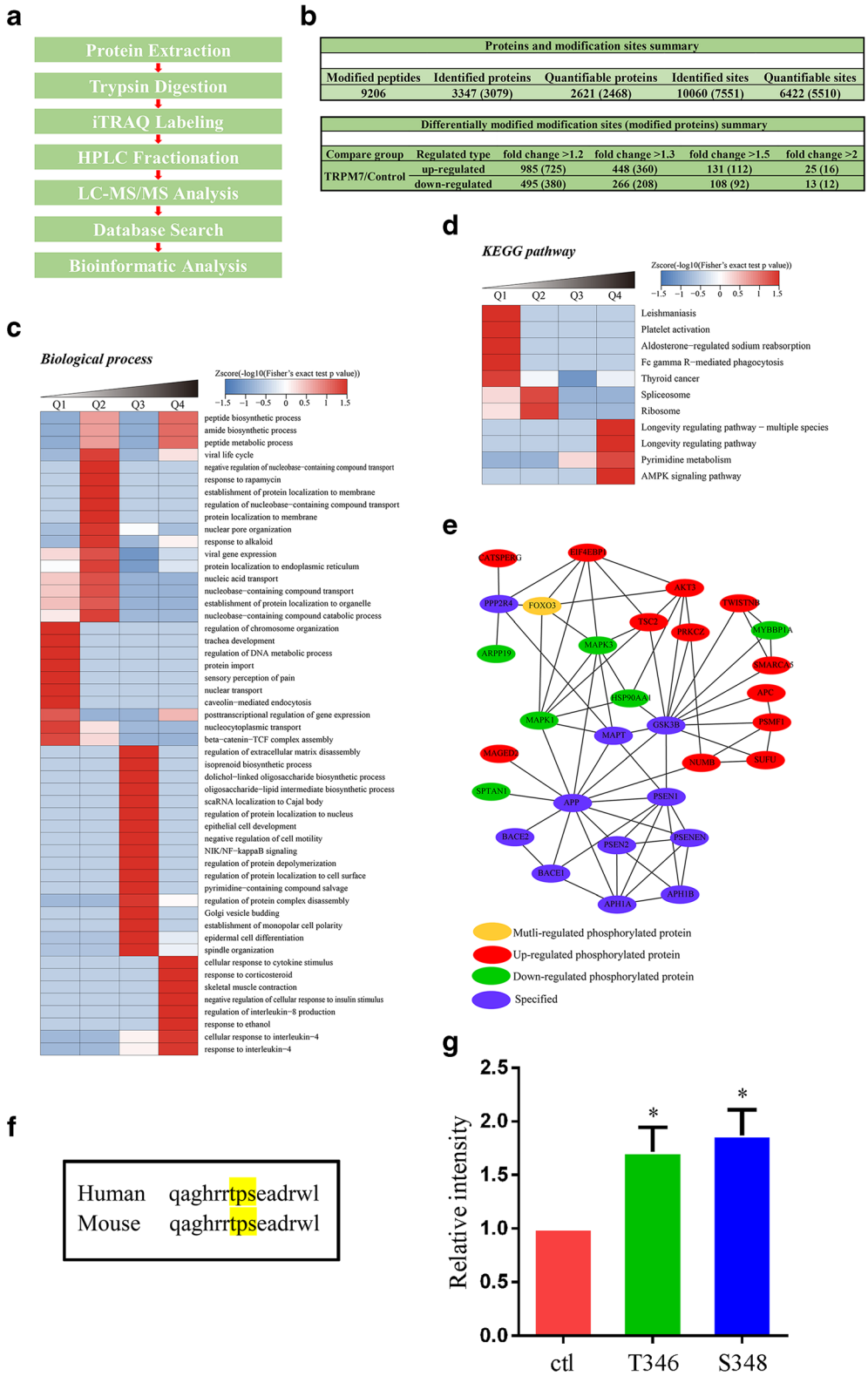
a
Protein Extraction
Trypsin Digestion
iTRAQ Labeling
HPLC Fractionation
LC-MS/MS Analysis
Database Search
Bioinformatic Analysis
b
Proteins and modification sites summary
Modified peptides 9206
Identified proteins 3347 (3079)
Quantifiable proteins 2621 (2468)
Identified sites 10060 (7551)
Quantifiable sites 6422 (5510)
Differentially modified modification sites (modified proteins) summary
Compare group Regulated type fold change >1.2 fold change >1.3 fold change >1.5 fold change >2
TRPM7/Control up-regulated 985 (725) 448 (360) 131 (112) 25 (16)
down-regulated 495 (380) 266 (208) 108 (92) 13 (12)
c
Biological process
Zscore(-log10(Fisher's exact test p value))
Q1 Q2 Q3 Q4
peptide biosynthetic process
amide biosynthetic process
peptide metabolic process
viral life cycle
negative regulation of nucleobase−containing compound transport
response to rapamycin
establishment of protein localization to membrane
regulation of nucleobase−containing compound transport
protein localization to membrane
nuclear pore organization
response to alkaloid
viral gene expression
protein localization to endoplasmic reticulum
nucleic acid transport
nucleobase−containing compound transport
establishment of protein localization to organelle
nucleobase−containing compound catabolic process
regulation of chromosome organization
trachea development
regulation of DNA metabolic process
protein import
sensory perception of pain
nuclear transport
caveolin−mediated endocytosis
posttranscriptional regulation of gene expression
nucleocytoplasmic transport
beta−catenin−TCF complex assembly
regulation of extracellular matrix disassembly
isoprenoid biosynthetic process
dolichol−linked oligosaccharide biosynthetic process
oligosaccharide−lipid intermediate biosynthetic process
scaRNA localization to Cajal body
regulation of protein localization to nucleus
epithelial cell development
negative regulation of cell motility
NIK/NF−kappaB signaling
regulation of protein depolymerization
regulation of protein localization to cell surface
pyrimidine−containing compound salvage
regulation of protein complex disassembly
Golgi vesicle budding
establishment of monopolar cell polarity
epidermal cell differentiation
spindle organization
cellular response to cytokine stimulus
response to corticosteroid
skeletal muscle contraction
negative regulation of cellular response to insulin stimulus
regulation of interleukin−8 production
response to ethanol
cellular response to interleukin−4
response to interleukin−4
d
KEGG pathway
Zscore(-log10(Fisher's exact test p value))
Q1 Q2 Q3 Q4
Leishmaniasis
Platelet activation
Aldosterone−regulated sodium reabsorption
Fc gamma R−mediated phagocytosis
Thyroid cancer
Spliceosome
Ribosome
Longevity regulating pathway − multiple species
Longevity regulating pathway
Pyrimidine metabolism
AMPK signaling pathway
e
CATSPER3
EIF4EBP1
AKT3
PPP2R4
FOXO3
TWISTNB
TSC2
PRKCZ
SYTL1BP1A
ARPP19
MAPK3
SMARCA5
HSP90AA1
APC
MAPK1
GSK3B
PSMF1
MAPT
MAGED2
NUMB
SUFU
SPTAN1
APP
PSEN1
BACE2
PSEN2
NSENEN
BACE1
APH1B
APH1A
Mutli-regulated phosphorylated protein
Up-regulated phosphorylated protein
Down-regulated phosphorylated protein
Specified
f
Human qaghrrtpseadrwl
Mouse qaghrrtpseadrwl
g
Relative intensity
2.5
2.0
1.5
1.0
0.5
0.0
*
*
ctl
T346
S348

◀ **Fig. 4** TRPM7 kinase overexpression regulated proteomic change and induces Numb phosphorylation. **a** Depiction of the iTRAQ experimental design workflow. **b** Statistics for proteins and modification sites in summary. **c** Heatmap for GO-based biological process analysis of upregulated (red) and downregulated (blue) proteins. **d** Heatmap for GO-based KEGG pathway analysis of upregulated (red) and downregulated (blue) proteins. **e** Target protein-protein interaction analysis of upregulated (red) and downregulated (green) proteins. **f** Comparison of the Numb sequences around the putative TRPM7 kinase phosphorylation site. The consensus sites are located at Thr346 and Ser348. **g** iTRAQ analysis of Numb Thr346 Ser348 phosphorylation intensity after TRPM7 kinase overexpression ($n = 3$). The data are presented as mean ± S.E.M. Unpaired Student's t test was used, $^*p < 0.05$ versus control

0.67. Group Q2 included proteins with fold change from 0.67 to 0.77. Group Q3 included proteins with fold change from 1.3 to 1.5. Group Q4 included proteins with fold change more than 1.5.

In Gene Ontology (GO) classification, we analyzed the biological process changes in response to TRPM7 α-kinase overexpression (Fig. 4c). A Kyoto Encyclopedia of Genes Genomes (KEGG) pathway–based analysis was performed to identify pathways that were potentially affected by the differential protein expression between TRPM7 α-kinase overexpression and control. The top pathways in response to TRPM7 α-kinase overexpression were the longevity regulating, pyrimidine metabolism, and AMPK signaling pathway (Fig. 4d). We then analyzed the relationship between Q4 proteins (fold change more than 1.5) and AD relative proteins. Eleven Aβ and tau pathway relative proteins (AD relative proteins) including APP, BACE1, BACE2, PSEN1, PSEN2, MAPT, APH1A, and APH1B (specified proteins) were selected. We found that 12 upregulated phosphorylated proteins (including Numb), 6 downregulated phosphorylated proteins, and 1 multi-regulated phosphorylated protein were associated with AD relative proteins (Fig. 4e).

To examine whether TRPM7 induces Numb phosphorylation, we transfected HEK293 cell with TRPM7 α-kinase plasmids and performed iTRAQ analysis. Comparisons between the protein sequences indicated that the 346TPS348 motif is conserved among human and mouse species (Fig. 4f). As shown in Fig. 4g, TRPM7 α-kinase overexpression increased Numb phosphorylation at Thr346 and Ser348 sites. These results suggest that TRPM7 α-kinase overexpression induced Numb phosphorylation, and show that the phosphorylated sites are Thr346 and Ser348.

CD82 overexpression promotes Aβ secretion via Numb phosphorylation

To examine whether CD82 induces Numb phosphorylation, we transfected HEK293 cell with CD82 plasmids and performed iTRAQ analysis. As shown in Fig. 5a, we identified 3203 proteins (2874 protein localization probability > 0.75) and 10,151 phosphorylation sites (8302 site localization probability > 0.75). We also quantified 2946 proteins (2792 protein localization probability > 0.75) and 7194 phosphorylation sites (5971 site localization probability > 0.75). Abundance of 113 phosphorylation sites and 99 proteins increased (fold change > 1.5), while abundance of 96 phosphorylation sites and 74 proteins decreased (fold change > 1.5) in response to CD82 overexpression.

In GO classification, we analyzed the biological process changes (Fig. 5b) and KEGG pathway changes (Fig. 5c) in response to CD82 overexpression. Then, we performed overlay analysis. We found that 11 proteins were upregulated in both TRPM7 α-kinase and CD82 overexpression (Fig. 5d). Furthermore, we showed that the levels of phosphorylated Numb were upregulated in the CD82 overexpression group (Fig. 5e). To explore the effect of CD82 on Aβ release, N2a/APP cells were transfected with CD82, or co-transfected with CD82 and Numb T346S348 mutation plasmids. As shown in Fig. 5f, g, CD82 overexpression increased $A\beta_{40}$ and $A\beta_{42}$ levels, which could be reversed by Numb T346S348 mutation.

Genetic deletion of *Cd82* may improve long-term memory in mice

Finally, we examined whether deletion of *Cd82* could rescue the hippocampal-related memory function. The grip strength test was used to evaluate motor function and deficits in control and $Cd82^{-/-}$ mice, which were characterized in our earlier study (Wei et al. 2014). Here we found that compared with normal control, $Cd82^{-/-}$ mice showed no difference in motor function (Fig. 6a). Motor skills and balance of our animals were assessed with the accelerating rotarod test. We found that $Cd82^{-/-}$ mice had the same motor skill and balance as the wild-type control animals (Fig. 6b). The radial arm water maze (RAWM) test and Y-maze test were used to assess

a

Proteins and modification sites summary				
Modified peptides	Identified proteins	Quantifiable proteins	Identified sites	Quantifiable sites
9873	3203 (2874)	2946 (2792)	10151 (8302)	7194 (5971)

Differencially modified modification sites (modified proteins) summary					
Compare group	Regulated type	fold change > 1.2	fold change > 1.3	fold change > 1.5	fold change > 2
CD82/Control	up-regulated	1021 (672)	413 (309)	113 (99)	17 (11)
	down-regulated	419 (343)	206 (166)	96 (74)	12 (9)

b

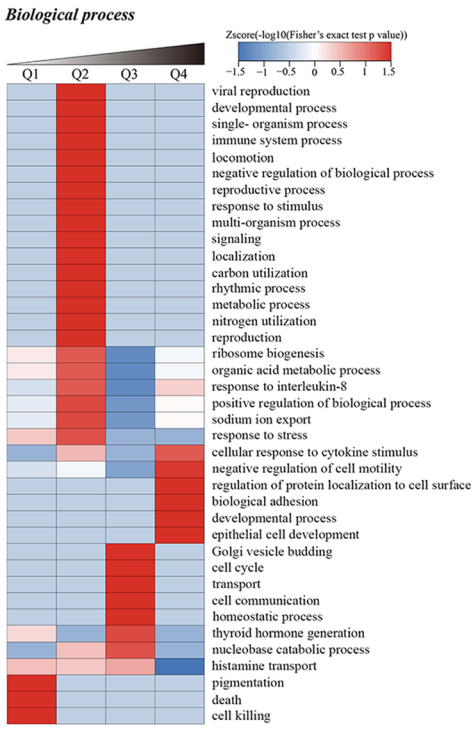

c

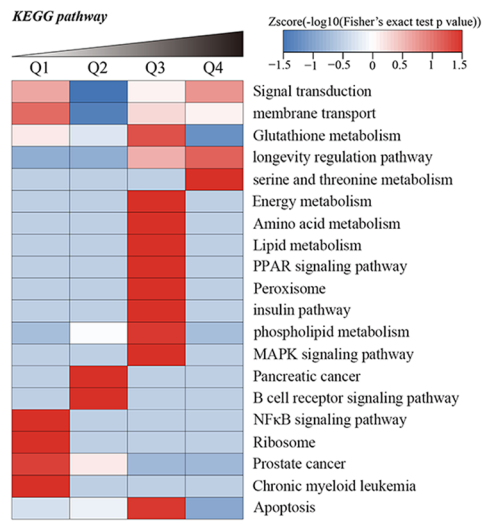

d

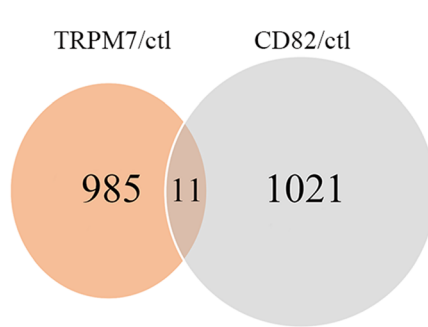

e

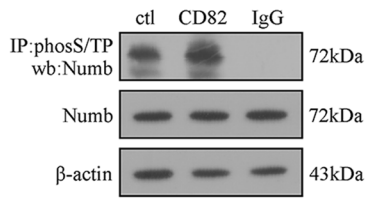

f

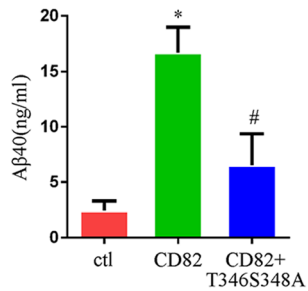

g

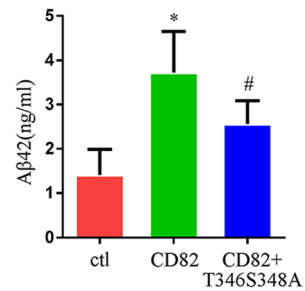

◀ **Fig. 5** CD82 increased Aβ secretion reduced by Numb phosphorylation mutation. **a** Summary statistics for proteins and modification sites after CD82 overexpression. **b** Heatmap for GO-based biological process analysis of upregulated (red) and downregulated (blue) proteins. **c** Heatmap for GO-based KEGG pathway analysis of upregulated (red) and downregulated (blue) proteins. **d** Overlay statistics for up-regulated proteins between TRPM7 kinase overexpression and CD82 overexpression group. **e** Western blotting analysis of phosphorylated Numb in CD82-overexpressing HEK293 cells ($n = 3$). **f**–**g** ELISA analysis of Aβ40 and Aβ42 secretion in CD82 and Numb phosphorylation mutation plasmids overexpressing N2a/APP cells ($n = 6$). One-way ANOVA with Bonferroni post hoc test was used. $^{*}p < 0.05$ compared with control; $^{\#}p < 0.05$ compared with CD82

hippocampus-related long-term memory deficits in *Cd82*$^{-/-}$ mice. We found that *Cd82*$^{-/-}$ mice took significantly less time to find the target than did the control mice during the probe phase (Fig. 6c, d). In addition, *Cd82*$^{-/-}$ mice made significantly fewer errors when finding the platform than did controls (Fig. 6e, f). During the Y-maze test, both wild-type and the *Cd82*$^{-/-}$ animals entered to the novel arms more often than to the familiar arm; however, the *Cd82*$^{-/-}$ mice entered the novel arm less often than the control mice (Fig. 6g). These findings suggested that genetic deletion of CD82 improved long-term memory in mice.

Discussion

Our study uncovered a potential novel signaling pathway of aging-induced pathological alterations in cognitive impairment. CD82 expression was increased in human AD brains and in middle-aged mouse models. CD82 overexpression impaired learning and memory in young adult mice. CD82 overexpression increased TRPM7 α-kinase cleavage via caspase-3 activation, then induced Numb phosphorylation at T346S348 sites. CD82-induced Aβ secretion depended on Numb phosphorylation. *Cd82*-knockout mice showed improved long-term memory. These findings suggest that elevated CD82-TRPM7 α-kinase-Numb signaling participates in age-related cognitive impairment and/or neurodegenerative diseases.

Tetraspanins are linked to various diseases; however, until now, the function of these proteins in neurodegeneration remains elusive. Tspan7 regulates glutamatergic and dopaminergic signaling through the trafficking of AMPA and dopaminergic receptor trafficking, respectively (Bassani et al. 2012; Lee et al. 2017). The AMPA and dopaminergic receptors regulate synapse assembly (Jacobi and von Engelhardt 2018) and neuronal circuits, and therefore the alterations of these receptors can cause neuronal disorders (Bassani et al. 2013; Rangel-Barajas et al. 2015).

In the present study, we found that CD82 overexpression impairs learning and memory in young adult mice and reduces spine density. The behavior changes caused by CD82 overexpression are similar to the early-stage neurodegenerative changes in AD and Parkinson's disease (Belghali et al. 2017; Callisaya et al. 2017). We extrapolate that CD82 overexpression impairs cognitive behavior by reducing spine density. Tspan6 is increased in AD brains, and Tspan6 overexpression increases APP-C-terminal fragments and $A\beta_{40}$ and $A\beta_{42}$ secretion (Guix et al. 2017). Notably, *Tspan6*-knockout mice show no changes in spine morphology or postsynaptic markers and therefore no defect in cognitive behavior (Salas et al. 2017). We found that *Cd82*-knockout improves long-term memory in mice, and we speculate that deletion of CD82 rescues the memory deficit which might be due to deactivation of the TRPM7-Numb pathway. However, there are some limitations in this study. First, we could examine the expression of CD82 in primary cultured neuron and in genetic model of AD (3xTg-AD mice), to confirm the changes in CD82 expression in vivo and in vitro. Second, by deleting *Cd82* in aged 3xTg-AD mice, we could confirm the role of CD82 in AD-like memory deficit. Third, we could upregulate and downregulate CD82 expression then examine the change of CD82-TRPM7-Numb pathway in primary cultured neuron. Finally, we could apply additional approaches, like laser speckle contrast imaging (Tarantini et al. 2017), to evaluate the effect of CD82 on memory deficit.

Our data showed that CD82 overexpression increases Numb phosphorylation and $A\beta_{40}$ and $A\beta_{42}$ secretion. Numb is an endocytic adapter protein that is crucial for amyloid precursor protein transport and processing (Chan et al. 2002; Kyriazis et al. 2008; Sun et al. 2016; Xie et al. 2012). We speculate that CD82 overexpression and increases in Aβ secretion are due to increased Numb activation which facilitates amyloid precursor protein processing and therefore impairs cognitive behavior.

TRPM7 is a dual-function membrane protein consisting of a TRP ion channel fused to an α-kinase

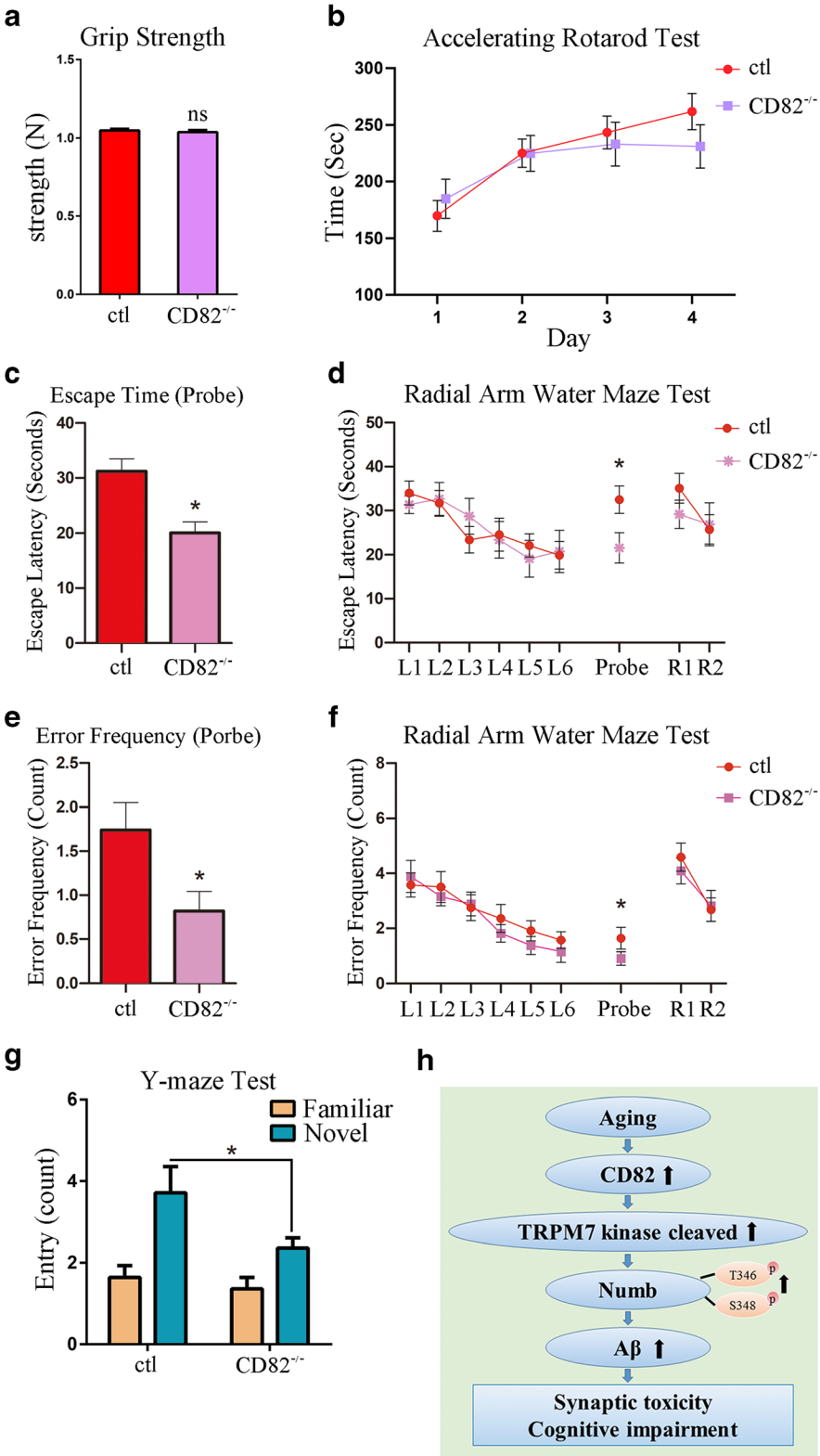
a
Grip Strength
strength (N)
ns
ctl
CD82-/-
b
Accelerating Rotarod Test
Time (Sec)
Day
ctl
CD82-/-
c
Escape Time (Probe)
Escape Latency (Seconds)
d
Radial Arm Water Maze Test
L1 L2 L3 L4 L5 L6 Probe R1 R2
e
Error Frequency (Porbe)
Error Frequency (Count)
f
Radial Arm Water Maze Test
g
Y-maze Test
Familiar
Novel
Entry (count)
h
Aging
CD82 ⬆
TRPM7 kinase cleaved ⬆
Numb
T346
S348
Aβ ⬆
Synaptic toxicity
Cognitive impairment

◀ **Fig. 6** *Cd82*$^{-/-}$ mice have improved hippocampal-related memory function. **a** To evaluate in vivo muscle strength and endurance, we determined forelimb grip strength using an electronic pull strain gauge. We found no significant difference between the wild-type ($n = 14$) and *Cd82*$^{-/-}$ animals ($n = 11$), Student's t test, $p = 0.536$. **b** The motor skill learning assessed by accelerating rotarod test. Both the wild-type ($n = 14$) and *Cd82*$^{-/-}$ animals ($n = 11$) remained on the wheel longer each day, but there was no significant difference between the two groups. Student's t test, day 1: $p = 0.4983$; day 2: $p = 0.9890$; day 3: $p = 0.6680$; day 4: $p = 0.2257$. Radial arm water maze test (RAWM) to assess hippocampal-related memory function showed that *Cd82*$^{-/-}$ animals had improved hippocampal-related long-term memory function compared with the wild-type animals. **c** *Cd82*$^{-/-}$ mice ($n = 10$) took significantly less time to find the target (escape time) compared with the control mice ($n = 14$) during the probe (probe only). **d** *Cd82*$^{-/-}$ mice took significantly less time to find the target (escape time) compared with the control mice during the probe (all time points plotted, Student's t test, $^*p = 0.0007$). **e** During the probe trials, *Cd82*$^{-/-}$ mice made significantly less errors finding the platform compared with controls (probe only). **f** During the probe trials, *Cd82*$^{-/-}$ mice made significantly less errors when finding the platform compared with controls (all time points plotted, Student's t test, $^*p = 0.0249$). **g** During the Y-maze test, both wild-type and the *Cd82*$^{-/-}$ animals entered to the novel arms more often than to the familiar arm. *Cd82*$^{-/-}$ animals entered into the novel arm less frequently than wild-type control animals. Student's t test, ctl novel vs. *Cd82*$^{-/-}$ novel: $^*p = 0.0315$; paired t test, ctl novel vs. ctl familiar: $^*p = 0.0002$ (not labeled on the plot), *Cd82*$^{-/-}$ novel vs. *Cd82*$^{-/-}$ familiar: $^*p = 0.0039$ (not labeled on the plot). **h** A schematic diagram for the role of CD82 in AD. CD82 is upregulated in aged mice. CD82 overexpression impairs memory ability and promotes TRPM7 kinase cleavage, leading to increased Numb phosphorylation and Aβ secretion

domain (Sun et al. 2015). Knockdown of TRPM7 expression with siRNA can inhibit Ca^{2+} uptake and accumulation in neurons and therefore protects anoxic neurons from ischemic stroke (Aarts et al. 2003). Additional studies found that a pharmacological inhibition of TRPM7 promotes pro-survival signaling and inhibits pro-apoptotic signaling in ischemic brain injury (Chen et al. 2015), and TRPM7 overexpression increases endoplasmic reticulum stress and neuronal cell apoptosis independent of its kinase activity (Huang et al. 2018). In the present study, we found that CD82 overexpression increases TRPM7 α-kinase cleavage, which then upregulates Numb phosphorylation and Aβ secretion. However, Liu and colleagues reported that TRPM7 knockdown in hippocampal neurons reduces structural synapse density, and restoring expression of the α-kinase domain in brains can rescue synapse plasticity and memory in TRPM7-knockout mice (Liu et al. 2018). This discrepancy might be induced by the dual function of TRPM7 α-kinase. Our previous study found that annexin A1 phosphorylated by TRPM7 α-kinase results in neuron apoptosis in ischemic stroke (Zhao et al. 2015). Others found that TRPM7 α-kinase could translocate to the nucleus and induce phosphorylation of histone H3 at serine 10, serine 28, and threonine 3 (Krapivinsky et al. 2014). During mitosis, phosphorylation of serine10 of histone H3 was accompanied with chromosome condensation (Prigent and Dimitrov 2003). In addition, histone H3 serine 28 mutation (H3S28A) present increases longevity and improve stress resistance in Drosophila models (Joos et al. 2018). These evidences indicate that TRPM7 α-kinase performs diverse functions independent of their channel function.

Overall, the present study provides evidence associating the CD82-TRPM7-Numb signaling with synaptic/memory dysfunction related to aging. Aging induces upregulated expression of CD82 and increases TRPM7 α-kinase cleavage and Numb phosphorylation, which promotes Aβ secretion (Fig. 6h).

Acknowledgments We thank Prof. Jiapei Dai from Chinese Brain Bank Center for providing human brain tissues, Prof. Jianzhi Wang from Key Laboratory of Ministry of Education for Neurological Disorders at Tongji Medical College of HUST for N2a/APP cell line, and Ms. Kathy Kyler of the University of Oklahoma Health Science Center for English editing.

Author contributions YZ, XL, AC, and XZ conceived and designed the project; YZ, TK, JD, LL, LZ, and XL performed the experiments; XZ, AC, ZU, and JS provided valuable advice, coordinated the studies, and/or conducted the data analysis; YZ, TK, and XZ wrote the manuscript with approval from all authors.

Funding information The current studies were supported by funding from the National Natural Science Foundation of China Grant No. 31800868 (to Dr. Yin Zhao).

Compliance with ethical standards

All animal experiments were approved by the Ethics Committees for Animal Experimentation of Huazhong University of Science and Technology and the University of Oklahoma Health Sciences Center in strict accordance with the Guide for the Care and Use of Laboratory Animals published by the U.S. National Institutes of Health. Efforts were made to minimize animal suffering and to reduce the number of animals used. This study was performed in accordance with the principles of the Declaration of Helsinki and approved by the Ethics Committee of Tongji Hospital, Tongji Medical College, HUST, China (2017-K-036).

Conflict of interest The authors declare that they have no conflicts of interest.

References

Aarts M, Iihara K, Wei WL, Xiong ZG, Arundine M, Cerwinski W, MacDonald J, Tymianski M (2003) A key role for TRPM7 channels in anoxic neuronal death. Cell 115(7): 863–877

Bassani S, Cingolani LA, Valnegri P, Folci A, Zapata J, Gianfelice A, Sala C, Goda Y, Passafaro M (2012) The X-linked intellectual disability protein TSPAN7 regulates excitatory synapse development and AMPAR trafficking. Neuron 73(6): 1143–1158. https://doi.org/10.1016/j.neuron.2012.01.021

Bassani S, Folci A, Zapata J, Passafaro M (2013) AMPAR trafficking in synapse maturation and plasticity. Cell Mol Life Sci 70(23):4411–4430. https://doi.org/10.1007/s00018-013-1309-1

Belghali M, Chastan N, Cignetti F, Davenne D, Decker LM (2017) Loss of gait control assessed by cognitive-motor dual-tasks: pros and cons in detecting people at risk of developing Alzheimer's and Parkinson's diseases. Geroscience 39(3): 305–329. https://doi.org/10.1007/s11357-017-9977-7

Callisaya ML, Launay CP, Srikanth VK, Verghese J, Allali G, Beauchet O (2017) Cognitive status, fast walking speed and walking speed reserve-the Gait and Alzheimer Interactions Tracking (GAIT) study. Geroscience 39(2):231–239. https://doi.org/10.1007/s11357-017-9973-y

Chan SL, Pedersen WA, Zhu H, Mattson MP (2002) Numb modifies neuronal vulnerability to amyloid beta-peptide in an isoform-specific manner by a mechanism involving altered calcium homeostasis: implications for neuronal death in Alzheimer's disease. NeuroMolecular Med 1(1):55–67. https://doi.org/10.1385/nmm:1:1:55

Charrin S, Jouannet S, Boucheix C, Rubinstein E (2014) Tetraspanins at a glance. J Cell Sci 127(Pt 17):3641–3648. https://doi.org/10.1242/jcs.154906

Chen W, Xu B, Xiao A, Liu L, Fang X, Liu R, Turlova E, Barszczyk A, Zhong X, Sun CL, Britto LR, Feng ZP, Sun HS (2015) TRPM7 inhibitor carvacrol protects brain from neonatal hypoxic-ischemic injury. Mol Brain 8:11. https://doi.org/10.1186/s13041-015-0102-5

Desai BN, Krapivinsky G, Navarro B, Krapivinsky L, Carter BC, Febvay S, Delling M, Penumaka A, Ramsey IS, Manasian Y, Clapham DE (2012) Cleavage of TRPM7 releases the kinase domain from the ion channel and regulates its participation in Fas-induced apoptosis. Dev Cell 22(6):1149–1162. https://doi.org/10.1016/j.devcel.2012.04.006

Fahlstrom A, Yu Q, Ulfhake B (2011) Behavioral changes in aging female C57BL/6 mice. Neurobiol Aging 32(10):1868–1880. https://doi.org/10.1016/j.neurobiolaging.2009.11.003

Feng J, Huang C, Wren JD, Wang DW, Yan J, Zhang J, Sun Y, Han X, Zhang XA (2015) Tetraspanin CD82: a suppressor of solid tumors and a modulator of membrane heterogeneity. Cancer Metastasis Rev 34(4):619–633. https://doi.org/10.1007/s10555-015-9585-x

Fleig A, Chubanov V (2014) TRPM7. Handb Exp Pharmacol 222: 521–546. https://doi.org/10.1007/978-3-642-54215-2_21

Forner S, Baglietto-Vargas D, Martini AC, Trujillo-Estrada L, LaFerla FM (2017) Synaptic impairment in Alzheimer's disease: a dysregulated symphony. Trends Neurosci 40(6): 347–357. https://doi.org/10.1016/j.tins.2017.04.002

Graham WV, Bonito-Oliva A, Sakmar TP (2017) Update on Alzheimer's disease therapy and prevention strategies. Annu Rev Med 68:413–430. https://doi.org/10.1146/annurev-med-042915-103753

Guix FX, Sannerud R, Berditchevski F, Arranz AM, Horre K, Snellinx A et al (2017) Tetraspanin 6: a pivotal protein of the multiple vesicular body determining exosome release and lysosomal degradation of amyloid precursor protein fragments. Mol Neurodegener 12(1):25. https://doi.org/10.1186/s13024-017-0165-0

Huang Y, Leng TD, Inoue K, Yang T, Liu M, Horgen FD et al (2018) TRPM7 channels play a role in high glucose-induced endoplasmic reticulum stress and neuronal cell apoptosis. J Biol Chem. https://doi.org/10.1074/jbc.RA117.001032

Jacobi E, von Engelhardt J (2018) AMPA receptor complex constituents: control of receptor assembly, membrane trafficking and subcellular localization. Mol Cell Neurosci. https://doi.org/10.1016/j.mcn.2018.05.008

Joos JP, Saadatmand AR, Schnabel C, Viktorinova I, Brand T, Kramer M et al (2018) Ectopic expression of S28A-mutated histone H3 modulates longevity, stress resistance and cardiac function in Drosophila. Sci Rep 8(1):2940. https://doi.org/10.1038/s41598-018-21372-3

Krapivinsky G, Krapivinsky L, Manasian Y, Clapham DE (2014) The TRPM7 chanzyme is cleaved to release a chromatin-modifying kinase. Cell 157(5):1061–1072. https://doi.org/10.1016/j.cell.2014.03.046

Kyriazis GA, Wei Z, Vandermey M, Jo DG, Xin O, Mattson MP, Chan SL (2008) Numb endocytic adapter proteins regulate the transport and processing of the amyloid precursor protein in an isoform-dependent manner: implications for Alzheimer disease pathogenesis. J Biol Chem 283(37):25492–25502. https://doi.org/10.1074/jbc.M802072200

Lee SA, Suh Y, Lee S, Jeong J, Kim SJ, Kim SJ, Park SK (2017) Functional expression of dopamine D2 receptor is regulated by tetraspanin 7-mediated postendocytic trafficking. FASEB J 31(6):2301–2313. https://doi.org/10.1096/fj.201600755RR

Liu Y, Chen C, Liu Y, Li W, Wang Z, Sun Q et al (2018) TRPM7 is required for normal synapse density, learning, and memory at different developmental stages. Cell Rep 23(12):3480–3491. https://doi.org/10.1016/j.celrep.2018.05.069

Prigent C, Dimitrov S (2003) Phosphorylation of serine 10 in histone H3, what for? J Cell Sci 116(Pt 18):3677–3685. https://doi.org/10.1242/jcs.00735

Rangel-Barajas C, Coronel I, Floran B (2015) Dopamine receptors and neurodegeneration. Aging Dis 6(5):349–368. https://doi.org/10.14336/ad.2015.0330

Salas IH, Callaerts-Vegh Z, Arranz AM, Guix FX, D'Hooge R, Esteban JA, de Strooper B, Dotti CG (2017) Tetraspanin 6: a novel regulator of hippocampal synaptic transmission and long term plasticity. PLoS One 12(2):e0171968. https://doi.org/10.1371/journal.pone.0171968

Shoji H, Miyakawa T (2019) Age-related behavioral changes from young to old age in male mice of a C57BL/6J strain

maintained under a genetic stability program. 39(2):100–118. https://doi.org/10.1002/npr2.12052

Sun Y, Sukumaran P, Schaar A, Singh BB (2015) TRPM7 and its role in neurodegenerative diseases. Channels (Austin) 9(5): 253–261. https://doi.org/10.1080/19336950.2015.1075675

Sun M, Asghar SZ, Zhang H (2016) The polarity protein Par3 regulates APP trafficking and processing through the endocytic adaptor protein Numb. Neurobiol Dis 93:1–11. https://doi.org/10.1016/j.nbd.2016.03.022

Tarantini S, Fulop GA, Kiss T, Farkas E, Zolei-Szenasi D, Galvan V et al (2017) Demonstration of impaired neurovascular coupling responses in TG2576 mouse model of Alzheimer's disease using functional laser speckle contrast imaging. Geroscience 39(4):465–473. https://doi.org/10.1007/s11357-017-9980-z

Tarantini S, Valcarcel-Ares NM, Yabluchanskiy A, Fulop GA, Hertelendy P, Gautam T, Farkas E, Perz A, Rabinovitch PS, Sonntag WE, Csiszar A, Ungvari Z (2018) Treatment with the mitochondrial-targeted antioxidant peptide SS-31 rescues neurovascular coupling responses and cerebrovascular endothelial function and improves cognition in aged mice. Aging Cell 17(2). https://doi.org/10.1111/acel.12731

Ungvari Z, Tarantini S, Hertelendy P, Valcarcel-Ares MN, Fulop GA, Logan S et al (2017) Cerebromicrovascular dysfunction predicts cognitive decline and gait abnormalities in a mouse model of whole brain irradiation-induced accelerated brain senescence. Geroscience 39(1):33–42. https://doi.org/10.1007/s11357-017-9964-z

Valcarcel-Ares MN, Tucsek Z, Kiss T, Giles CB, Tarantini S, Yabluchanskiy A, Balasubramanian P, Gautam T, Galvan V, Ballabh P, Richardson A, Freeman WM, Wren JD, Deak F, Ungvari Z, Csiszar A (2019) Obesity in aging exacerbates neuroinflammation, dysregulating synaptic function-related genes and altering eicosanoid synthesis in the mouse hippocampus: potential role in impaired synaptic plasticity and cognitive decline. J Gerontol A Biol Sci Med Sci 74(3): 290–298. https://doi.org/10.1093/gerona/gly127

Visser D, Middelbeek J, van Leeuwen FN, Jalink K (2014) Function and regulation of the channel-kinase TRPM7 in health and disease. Eur J Cell Biol 93(10–12):455–465. https://doi.org/10.1016/j.ejcb.2014.07.001

Wang XC, Zhang YC, Chatterjie N, Grundke-Iqbal I, Iqbal K, Wang JZ (2008) Effect of melatonin and melatonylvalpromide on beta-amyloid and neurofilaments in N2a cells. Neurochem Res 33(6):1138–1144. https://doi.org/10.1007/s11064-007-9563-y

Wei Q, Zhang F, Richardson MM, Roy NH, Rodgers W, Liu Y, Zhao W, Fu C, Ding Y, Huang C, Chen Y, Sun Y, Ding L, Hu Y, Ma JX, Boulton ME, Pasula S, Wren JD, Tanaka S, Huang X, Thali M, Hämmerling GJ, Zhang XA (2014) CD82 restrains pathological angiogenesis by altering lipid raft clustering and CD44 trafficking in endothelial cells. Circulation 130(17):1493–1504. https://doi.org/10.1161/circulationaha.114.011096

Xie Z, Dong Y, Maeda U, Xia W, Tanzi RE (2012) RNAi-mediated knock-down of Dab and Numb attenuate Abeta levels via gamma-secretase mediated APP processing. Transl Neurodegener 1(1):8. https://doi.org/10.1186/2047-9158-1-8

Yap CC, Winckler B (2015) Adapting for endocytosis: roles for endocytic sorting adaptors in directing neural development. Front Cell Neurosci 9:119. https://doi.org/10.3389/fncel.2015.00119

Zhao Y, Wang J, Jiang H, Yu Z, Li X, Shi J (2015) Following OGD/R, annexin 1 nuclear translocation and subsequent induction of apoptosis in neurons are assisted by myosin IIA in a TRPM7 kinase-dependent manner. Mol Neurobiol 51(2):729–742. https://doi.org/10.1007/s12035-014-8781-y